Geophys. J. Int. (2006) **166,** 839–854 doi: 10.1111/j.1365-246X.2006.03073.x

Amplitude spectra moment tensor inversion of shallow earthquakes in Spain

S. Cesca,[1,2,*] E. Buforn[1] and T. Dahm[2]

[1]*Department Geofisica y Meteorologia, Universidad Complutense Madrid, Spain*
[2]*Institut für Geophysik, University of Hamburg, Germany*

Accepted 2006 May 16. Received 2006 April 13; in original form 2005 December 2

SUMMARY

The study of focal mechanisms for shallow earthquakes of low-to-moderate magnitude at regional distances requires a proper inversion technique. One of the major problems is the correct separation of path effects from source effects. The method used should take into account problems arising from errors in the definition of crustal structure and inclusion of the high-frequency content of the waveforms. In this study a method of frequency domain moment tensor inversion to determine deviatoric moment tensor solutions from body wave amplitude spectra is described. The method has been tested with synthetic data to define instabilities that are due to mismodelling of several parameters. The inversion technique is applied to broadband seismic data of shallow (10 km depth) earthquakes in Spain. Solutions are obtained for a range of depths and compared with solutions obtained with different methods, such as first motion polarities and moment tensor inversion in the time domain. A combined fit of amplitude spectra, first motion polarities and double-couple component is introduced as a method which resolves better the non-uniqueness of solution. The proposed method can be implemented in fast moment tensor inversion when a Green functions database has been created in advance for the studied area.

Key words: earthquake-source mechanism, inversion, seismic moment, seismology.

1 INTRODUCTION

The seismicity of Spain is characterized by the occurrence of mostly shallow ($h < 35$ km) earthquakes of low-to-moderate magnitude ($M_w < 5.0$). The most active seismic regions are located in southern Spain and Alboran Sea, mainly related to NW–SE convergence along the plate boundary between Eurasia and Africa (Udías *et al.* 1976; Buforn *et al.* 1988, 1995, 2004; Calvert *et al.* 2000; Jiménez-Munt & Negredo 2003). Intermediate and deep earthquakes also occur in this region (Hatzfeld 1978; Buforn *et al.* 1991, 1997, 2004; Morales *et al.* 1999). The Pyrenees region is characterized by small earthquakes at shallow depth (Souriau & Pauchet 1998; Goula *et al.* 1999). Owing to the small average magnitude of the earthquakes, focal mechanism solutions are rarely available from regional or global moment tensor projects. Intermediate and deep earthquakes in Spain have been studied in more detail (Buforn *et al.* 1997; Coca 1999), while the analysis of shallow events has been approached only recently for Ibero-Maghreb region (Stich *et al.* 2003; Rueda & Mézcua 2005). Moment tensor inversion for shallow weak events ($Ml < 4.5$) is often difficult owing to the high-frequency or short-wavelength radiation and thus the possible mismodelling of crustal structure.

A common approach in moment tensor inversion is the comparison of observed and synthetic seismograms in the time domain (Dziewonski *et al.* 1981; Dreger & Helmberger 1993). This method is more stable when it is applied to long-period, long-wavelength data; it is used in most of fast moment tensor projects, both on a global (e.g. Harvard CMT, Dziewonski & Woodhouse 1983; USGS, Sipkin & Needham 1993; Tokio University, Kawakatsu 1995; etc.) or on a regional scale (ETHZ, Braunmiller *et al.* 2002; MedNet, Pondrelli *et al.* 2002; IAG, Stich *et al.* 2003; Instituto Geografico Nacional of Spain, IGN, Rueda & Mezcua 2005; etc.). These methods often use either the whole waveforms or the surface waves. At wavelengths longer than the scale of major crustal heterogeneities or surface topography, this approach is quite stable even when averaged 1-D earth models are used. Nevertheless, small earthquakes do not generate energetic long-period waves and at higher frequencies unconsidered crustal heterogeneities may influence the results. Owing to these problems, regional moment tensor inversions are rarely applied to small events, the magnitude threshold typically ranging from 4.5 (ETHZ, MedNet) to 5.5 (Harvard, USGS). An important improvement of moment tensor inversion technique applicability is due to Stich *et al.* (2003), who have substantially reduced these thresholds, being able to retrieve moment tensors of smaller events ($M_w \geq 3.5$) when surface waves are sufficiently excited.

*Corresponding author: Institut für Geophysik, Universität Hamburg, Bundesstrasse 55, D-20146, Hamburg, Germany. E-mail: cesca@dkrz.de.

In this study, we have developed a method of amplitude spectra moment tensor inversion for the determination of focal mechanism from shallow and weak regional earthquakes with the attempt to resolve the instability and biasing problem at higher frequencies up to about 5 Hz. We use body wave data from broad-band stations at regional distances, considering both *P* and *S* waves. Method instabilities have been checked by a set of tests using theoretical data. The technique has been applied to seven significant events in Spain and results have been compared with other studies and with first motion polarity solutions. One important aspect is that different misfit criteria have been tested to remove possible non-uniqueness for sparse data sets.

2 METHODOLOGY

Moment tensor inversion requires the a priori determination of theoretical displacements from the earthquake on the Earth's free surface. The general representation of displacement u_n, with component n, may be simplified by the following equation (Aki & Richards 1980; Udias 1999; summation convention applied, $n = 1, 2, 3$):

$$u_n(t) = \int m_{pq} {}^{*} G_{np,q}\, dA. \tag{1}$$

The moment tensor density, m_{pq}, depends on slip and fault orientation, while the spatial derivatives of the Green functions, $G_{np,q}$, represent the wave propagation and depend on the earth model and geometry. The integration is carried out over the rupture plane A; * denotes time convolution.

Using the further approximation of point source and far field, and considering only the first order terms of Green functions around the centroid location, we may write equation 1 in the frequency domain in the following matrix form:

$$u_n(\omega) = s(\omega) A_{nj}(\omega) f_j, \quad j = 1, 6. \tag{2}$$

The spectrum of the displacement $u(\omega)$ is expressed as a sum of six weighted elementary seismograms $A_{nj}(\omega)$ the centroid source time function STF $s(\omega)$, and scalars f_j . f_j represent the amplitudes of basic seismic dipole sources or couples. The STF term represents the slip rate at the source (fault). We have used a smoothed triangle function with length T in the time domain, so that in the frequency domain we have a flat spectrum below the corner frequency of 1/T and a 3 dB slope (Brüstle & Müller 1983). The choice of a 1-D model reduces the set of 18 elementary seismograms to only 8 independent ones, 3 for the vertical and radial motion and 2 for the transverse one. Therefore, to obtain the synthetic seismograms, one has to add the spectra of eight independent elementary seismograms, weighted by factors f depending on seismic moment tensor components. The equation for the amplitude spectra of the displacement is not linear and it is given by:

$$|u_n(\omega)| = \sqrt{[\Re(s A_{nj} f_j)]^2 + [\Im(s A_{nj} f_j)]^2}, \tag{3}$$

where $\Re$ and $\Im$ indicate real and imaginary components.

In this study, the reflectivity method (Müller 1985) has been used for the determination of the Green functions, or elementary seismograms, which are obtained in the frequency domain as integrals over horizontal slownesses (Koch 1991; Dahm & Krüger 1999; Cesca 2005). In a second step, we estimated synthetic seismograms from eq. (2). The reflectivity method requires the definition of a flat horizontally layered earth model, consistent with its application within regional distances (less than 350 km); it also requires the location of the station network and some characteristics of the source. The earth model has to be described by defining the rheological parameters, such as density, *P* and *S* wave velocities and attenuation coefficients, as well as the geometry of layering. When dealing with body waves only it is possible to consider different source and receiver structures (e.g. new version of code from Wang 1999). The source depth must be also specified to calculate the Green functions. However, it is possible to estimate this parameter by comparing inversion results from different sets of Green functions corresponding to a range of focal depths.

After the Green functions have been calculated, the non-linear inversion is iteratively solved by a gradient method (Gauss method) using a starting model and L_2-norm. A possible problem of a gradient method is that the solution may stick near a local minimum. Therefore, the inversion procedure is based on a systematic grid walk from 729 starting solutions, which are disposed in a 6-D space around an arbitrary initial configuration of the moment tensor. As a first step, time windows for the data and Green functions are selected. Both observed and synthetic seismograms are tapered in the time domain. The Fourier transform is applied to a properly enlarged time window. The frequency sampling rate is defined in function of the number of points and the data sampling of time windows, as the inverse of the time window length. Data are then filtered in frequency domain with an acausal bandpass filter. The amplitude spectra inversion is then carried out, the misfit between observed and synthetics being expressed as:

$$\text{misfit} = \frac{\sum w_j^2 \left(d_j^{\text{syn}} - d_j^{\text{obs}}\right)^2}{\sum w_j^2 \left(d_j^{\text{obs}}\right)^2}, \tag{4}$$

where w_j, d_j^{syn}, d_j^{obs} are, respectively, the weighting factor, synthetic and observed data corresponding to the *j*th sample. *d* is either vertical, radial or transversal component of displacement. The advantage of working in frequency domain lies in the higher stability and lower dependence on alignment of the observed seismograms and Green functions. On the other hand, a solution obtained in the frequency domain looses information about phases and is, therefore, ambiguous in the sense that pressure and tension axis can not be distinguished. Time shifts to maximize the cross-correlation between observed and synthetics seismograms are then estimated for the best amplitude spectra inversion result, and the sign of the cross-correlation factor is used to distinguish the pressure and tension axis. When synthetic seismograms show a poor correlation with data, the ambiguity between pressure and tension axis can still be resolved by checking the fit of the observed first motion polarities. We estimated the source depth by comparing misfits of inversion solutions, assuming different depths. The STF time length was found in the following step, when we repeated the inversion, fixing the source depth and considering different STF durations. As will be shown in the synthetic tests section, this procedure may help to constrain better the scalar seismic moment; it is stable in terms of the focal mechanisms retrieved. The proposed inversion method is especially flexible, allowing the inversion in either the time domain or the frequency domain, allowing either time traces or amplitude spectra to be fitted, or, in a mixed approach, time traces and spectra to be fitted at the same time. Others powerful tools of our method include the possibility of applying different bandpass filters to different data traces (e.g. for body and surface waves) and the application of an individual weight for each trace. In reference to the inverted moment tensor, this method allows to put several constraints on the source mechanism: pure double couple, null isotropic component solution (DC+CLVD), general dislocation (see Dahm *et al.* 1999, eq. 3) or pure tensile source.

In this study the inversion has been carried out using only data windows corresponding to body waves. This choice results in a more generalized approach, which can be applied to both shallow and intermediate depth earthquakes. In detail, vertical and radial components of *P* waves and transverse components of *S* waves have been used. The application to seismic data at regional distances for shallow events implies that fitted phases correspond either to direct waves or to critical refractions. A double weight is given to *P* arrivals with respect to *S* peaks and a distance dependent weight is applied to all data, in order to increase the weight of stations which are located further from the epicentre and show, therefore, lower amplitudes. The same bandpass filter is applied both to the data and to the Green functions, the frequency range being between 0.1 and 2 Hz. We have used different values, between 0.5 and 4 Hz, when studying events with magnitude lower than $M_W = 4$. Crustal layers have been modelled by using averaged values of attenuations coefficients ($Q_a = 400$, $Q_b = 200$), which have been estimated for the region studied (Pujades *et al.* 1990). Time windows for Green functions and data are defined in agreement with theoretical arrival times and phase picking. Frequency domain inversion is then carried out and best moment tensor calculated. The inversion solution is given here in terms of five independent components of the moment tensor, and constraining the isotropic component to be zero. This constraint is reasonable for tectonic earthquakes, but not for volcanic shocks. The deviatoric moment tensor solution is decomposed in a DC term and a compensated linear vector dipole, CLVD (see Jost & Hermann 1989). CLVD is defined from the eigenvalues of the deviatoric moment tensor (Dziewonski *et al.* 1981) as follows:

$$\mathrm{CLVD} = \left| \frac{m_{\min}}{m_{\max}} \right|. \tag{5}$$

In this equation $m_{\min}$ and $m_{\max}$ are deviatoric eigenvalue in the absolute sense (e.g. Jost & Hermann 1989). The percentage of CLVD is calculated for the different solutions obtained and considered as an indicator of the quality of the results.

A problematic point in the determination of the moment tensor is related to the non-linearity of the inversion procedure. The main consequence of this is the necessity to include in the inversion method a recursive algorithm which allows the evaluation of moment tensor solutions for a wide set of initial configurations. The solution analysis by considering different parameters can improve the identification of the best solution. As we will show in the next paragraphs, with data from shallow earthquakes, the interpretation of results can be difficult (non-unique) and there can be different possible solutions. A typical approach to solve this ambiguity is to select the best fitting solution, that is to say, the one minimizing the misfit between the observed and theoretical amplitude spectra. Following this procedure, we analysed the space of possible solutions for each source depth considered. We considered as a possible solution each inversion result which has a misfit up to 15 per cent higher than the minimum misfit for the same depth. Nevertheless, our experience suggests a more careful analysis of the results and considering other important parameters, such as the fit of the observed first motion polarities and a reduced percentage of the CLVD component, which help in defining the goodness of moment tensor solution. We have, therefore, introduced a new parameter, here defined as combined misfit (CM), to distinguish the best solution of the moment tensor inversion. This CM is weighted on the fit of amplitude spectra, first motion polarities and the DC percentage of the focal mechanism. We stress that the inclusion of the CLVD percentage in the misfit estimation is considered an assumption. Still, we consider this to be a reasonable and useful approach, at least when studying focal mechanisms of small-to-moderate tectonic earthquakes, for which the estimation of the non-DC component is unusual. The combined misfit is expressed by the following equation:

$$\mathrm{CM} = 0.5\left(\frac{\text{Misfit-Min.misfit}}{\text{Min.misfit}}\right) + 0.25\left(\frac{\mathrm{CLVD}}{100}\right) + 0.25\left(\frac{\text{Wrong polarities}}{\text{Total observed polarities}}\right). \tag{6}$$

3 SYNTHETIC TESTS

Before applying the method to observed earthquakes, we carried out several synthetic tests in order to evaluate the stability of the inversion procedure. We gave a special attention to four parameters: the earth model layering, the focal depth, the STF duration and the azimuthal coverage. To carry out these tests, we first obtained synthetic data sets for two layered models, which represented simple models of the crustal structure over an homogeneous litosphere. Model M2 (Fig. 1a) is composed by one homogeneous layer over a half-space and model M3 (Fig. 1b) reproduces a three-layered crust over a half-space. Results corresponding to a normal fault source

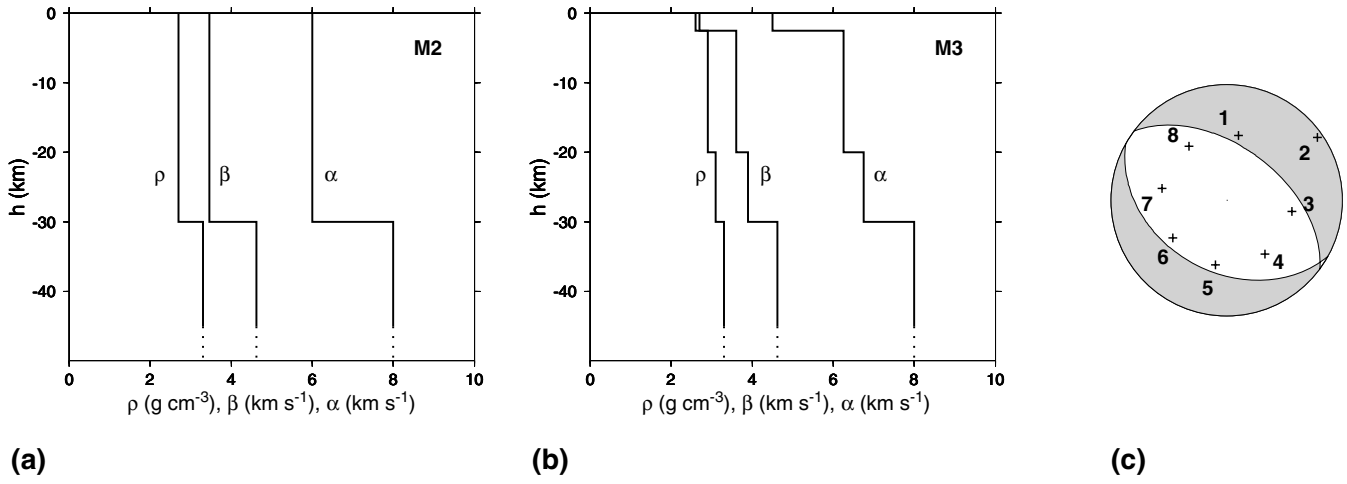

Figure 1. Earth models used for the synthetic tests of inversion: model M2 (a) and model M3 (b) are described by density (ρ), *P*-wave velocity (α) and *S*-wave velocity (β). Fault plane solutions (c) was used to generate synthetic data. Crosses represent station distribution.

mechanism (strike $\varphi = 118^\circ$, dip $\delta = 39^\circ$ and slip $\lambda = -96^\circ$) of pure DC (Fig. 1c) are shown. The source depth is fixed at 10 km, the STF duration is 0.5 s and the scalar seismic moment is $M_0 = 1.0 \times 10^{17}$ N m. Theoretical seismograms were obtained for eight stations (Fig. 1c) with epicentral distances between 100 and 220 km with good azimuthal coverage. In the following tests, the inversions were carried out using theoretical Green functions, which considered different errors in the model in accordance with the four parameters previously described. Briefly, we present these results with major attention to the behaviour observed at a common station (STA2).

3.1 Earth model

The first set of tests has been carried out to check the inversion when a wrong earth model has been used to estimate Green functions. These tests are especially important in order to estimate possible anomalies of moment tensor inversion when using an incorrect crustal structure. Such a situation is likely to occur when dealing with shallow earthquakes, owing to the poor knowledge of crustal structure, the existence of different models for the area and the simplification we introduce by assuming a 1-D model. First we use model M2 to generate the data and consider model M3 to generate theoretical Green functions, according to the inversion scheme just described. Results of the inversion (Fig. 2) show a wrong determination of the moment tensor in terms of fault plane orientation (strike $\varphi = 94^\circ$, dip $\delta = 31^\circ$ and slip $\lambda = -138^\circ$ versus the correct values of $\varphi = 118^\circ$, $\delta = 39^\circ$, $\lambda = -96^\circ$), but a low component of CLVD (6 per cent). The poor determination of the moment tensor corresponds to a poor fit between theoretical (grey areas) and observed (black lines) spectra, which is shown in Fig. 2, relatively to vertical components of *P* waves and transverse components of *S* waves. Observed amplitude spectra are characterized by the strong heterogeneity at the base of the crust and are directly related to the epicentral distance. These considerations explain the shape of the spectra and the similarity, for example, between spectra of stations STA1, STA4 and STA7, which have the same epicentral distance of 180 km. With respect to the model used to generate data, model M3 is characterized by major layer complexity and the smoother variation of reological parameters with depth. These characteristics result in smaller amplitudes of isolated phases and in an increase of reverberation and coda energy, explaining therefore the smoothness of theoretical amplitude spectra. The plot of theoretical (thin lines) and observed (thick lines) displacements shows important differences, which are observed as a consequence of the different crustal layering. Analysing in detail the comparison of displacements at the reference station STA2, we can observe the fit of the first motion polarities, but the amplitudes

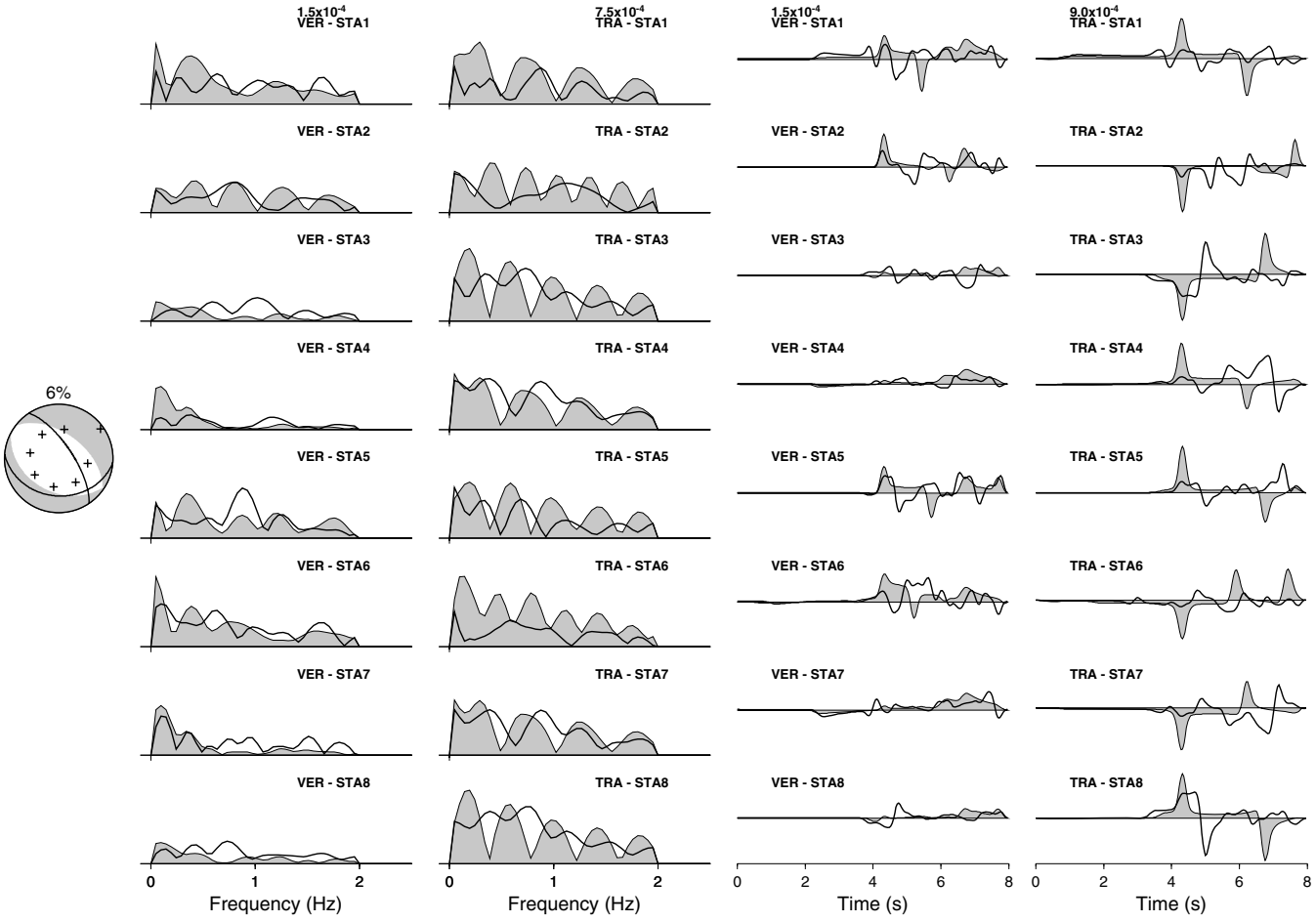

Figure 2. Results of moment tensor inversion for wrong definition of earth model. Synthetic data have been generated with model M2 and Green functions with model M3. Left: focal mechanism to generate synthetic data (grey focal sphere), focal mechanism of DC component of solution (black lines), CLVD percentage of solution and distribution of stations (crosses). Right: comparison of data (grey areas) and theoretical resulting from amplitude spectra moment tensor inversion (black lines). The figure shows the comparison of amplitude spectra and seismograms, corresponding to vertical *P* wave and transverse *S* wave at the eight stations used. Amplitudes are rescaled to a common epicentral distance of 100 km and normalized by coefficients shown at the top of each column.

of observed phases and their fit through the whole data windows can not be reproduced correctly. More rarely, errors in the obtained solution result in a wrong determination of first motion polarities (for example, observed for the vertical component of STA3). When model M3 was used to generate synthetic data and model M2 for Green functions, the result shows a correct fault plane solution, but a large anomalous CLVD component (39 per cent). The wide range of tests that have been carried out with different earth models show that in general a layered model better reproduces other layered model, while the inversion is more unstable when a gradient velocity model is used to estimate the Green functions. On the other hand, similar results were obtained when different source mechanisms were used to calculate synthetic data (strike-slip, normal, reverse and vertical fault), showing how these conclusions are valid independently of the characteristics of the focal mechanism (Cesca 2005).

3.2 Focal depth

A second set of synthetic tests studied the influence of the source depth definition. Synthetic data were generated using model M2 and a source depth of 10 km, while Green functions were obtained with the same model and for depths of 5, 10, 22 and 40 km. The main results are shown in Fig. 3, together with the fit of amplitude spectra and the comparison of observed and theoretical seismograms, again for station STA2. Also in this case, the possibility of retrieving the correct solution strongly depends on the accuracy in source depth definition, and better solutions are obtained when approaching the correct source depth of 10 km. Major instabilities were observed when the source was getting closer to the free surface ($h = 5$ km) and when it was embedded in a different layer ($h = 40$ km). The shallow source solution ($h = 5$ km) is characterized by anomalous percentage of CLVD, estimated in 52 per cent. However, the fault plane orientation obtained was very close to the correct solution. The retrieval of an high non-DC component was observed also when considering different earth models and seems to indicate some instability in the inversion method when sources are very close to the free surface, with a depth less than 5 km. The comparison of observed and theoretical seismograms for the vertical component (Fig. 3) is characterized by the fit of first arrivals, while the following phases present a worse fit, as the error in source depth definition introduces an offset between theoretical and observed arrival times. Considering sources deeper than 10 km, we observed how the solution got progressively worse when increasing the source depth. In the most extreme case considered ($h = 40$ km), the solution was incorrect both in terms of the fault plane ($\varphi = 352^\circ$, $\delta = 60^\circ$, $\lambda = 3^\circ$ versus $\varphi = 118^\circ$, $\delta = 39^\circ$, $\lambda = -96^\circ$) and of the percentage of CLVD (39 per cent). In this case the erroneous result was a consequence both of the wrong depth definition and of the fact that the source was embedded in a different layer.

3.3 STF duration

The third test (Fig. 4) studies the effects of a change in source time function duration. For this test a set of Green functions was calculated for the following STF durations: 0.20, 0.35, 0.50, 0.75 and 1.00 s, while data were obtained for a STF of 0.50 s. Both Green functions and data correspond to model M3 and $h = 10$ km. The inversion procedure was very stable over a wide range of STF lengths, which range from about half to the double of the correct value of 0.5 s, and good solution were obtained for all tests: the variation of fault plane angles was lower than 3°, the percentage of CLVD lower than 6 per cent. The quality of results was confirmed by the good fit between synthetic and observed spectra, as well as by the comparison of observed and synthetic seismograms (shown in Fig. 4 for station STA2). For the largest STF (1.00 s) an important effect was related to changes in the waveform characteristics: two pulses could be observed in the vertical component of observed seismograms at the first arrival versus a single larger pulse on the synthetics. Major effects of the mismodelling of the STF length were in the wrong determination of the scalar seismic moment,

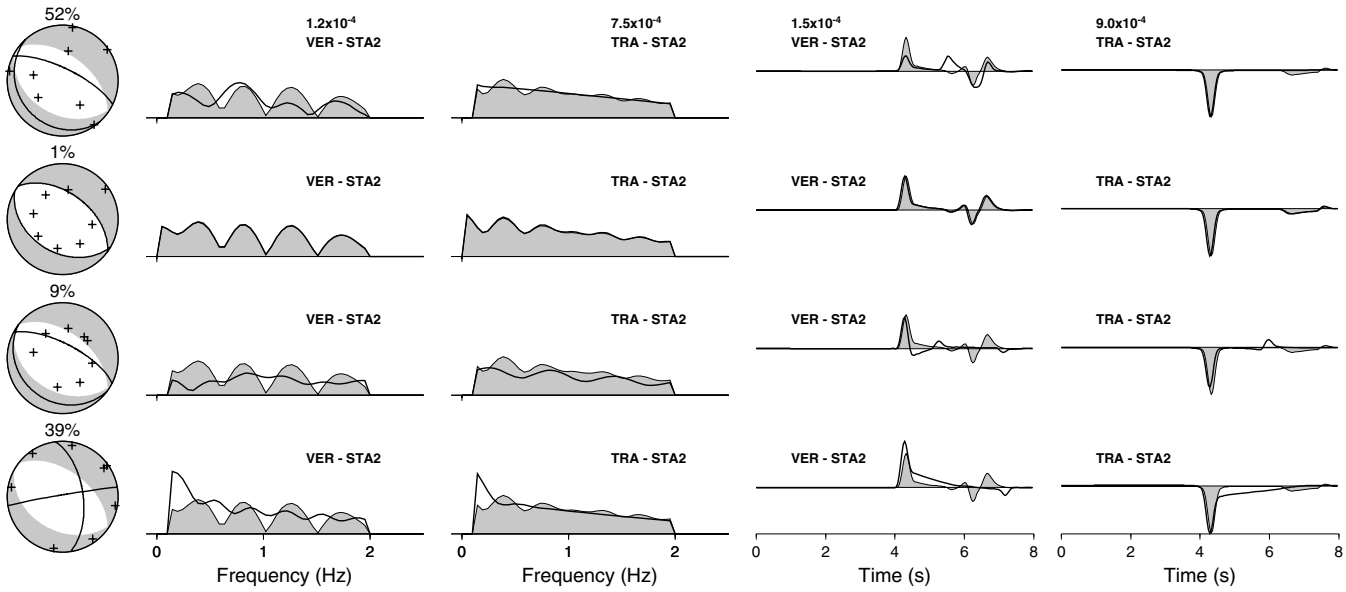

Figure 3. Results of moment tensor inversion for wrong definition of source depth. Synthetic data have been generated with model M2 and $h = 10$ km, Green functions with same model and source depths of 5, 10, 22 and 40 km (from top to bottom). Left: focal mechanism to generate synthetic data (grey focal sphere), focal mechanism of DC component of solution (black lines), CLVD percentage of solution and distribution of stations (crosses). Right: comparison of observed (grey areas) and theoretical (black lines) spectra and seismograms, corresponding to vertical *P* wave and transverse *S* wave at station STA2. Amplitudes are rescaled to a common epicentral distance of 100 km and normalized by coefficients shown at the top of each column.

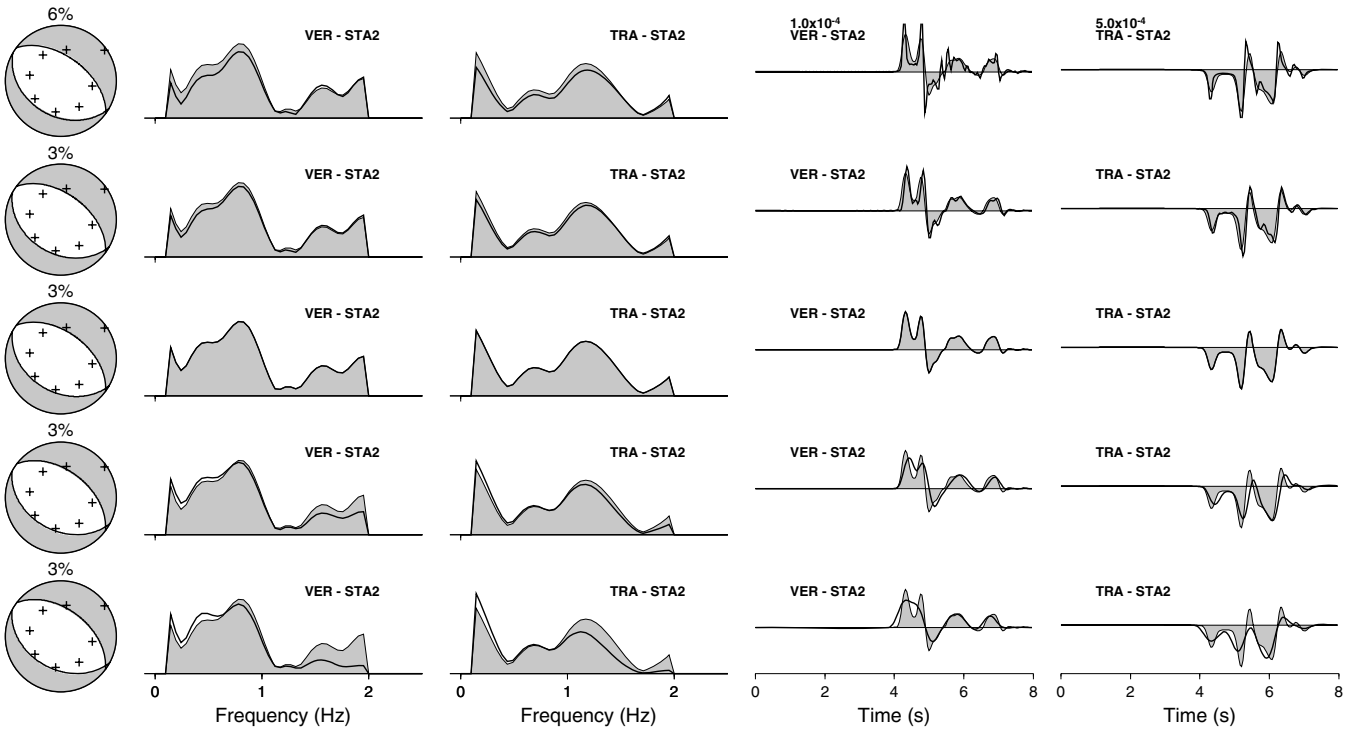

Figure 4. Results of moment tensor inversion for wrong definition of STF duration. Synthetic data have been generated with model M3, $h = 10$ km and STF of 0.50 s, Green functions with the same model and STF of 0.20, 0.35, 0.50, 0.75 and 1.00 s. Left: focal mechanism to generate synthetic data (grey focal sphere), focal mechanism of DC component of solution (black lines), CLVD percentage of solution and distribution of stations (crosses). Right: comparison of observed (grey areas) and theoretical (black lines) spectra and seismograms, corresponding to vertical *P* wave and transverse *S* wave at station STA2. Amplitudes are rescaled to a common epicentral distance of 100 km and normalization by coefficients shown at the top of each column.

the value of which (the correct one being 1.0×10^{15} N m) grew while increasing STF length from 0.8×10^{15} to 1.2×10^{15} N m. Such an effect is due simply to the equivalence between the scalar seismic moment and the integral of STF. Let us consider the case of choosing a shorter STF, with respect to the correct one. If we maintain unchanged the value of scalar moment, we will constrain the STF to have a higher amplitude and, therefore, obtain higher amplitudes in the synthetic seismograms. To fit smaller amplitudes of the data, the inversion procedure will, therefore, estimate a smaller scalar moment.

3.4 Azimuthal coverage

Finally, the effects of a poor distribution of seismic stations have been studied. The synthetic tests commented on before were repeated while reducing the azimuthal coverage: from the optimal situation with eight stations with an uniform distribution around the epicentre, these were progressively reduced to four stations with an azimuthal coverage of 50 per cent. The reduction of azimuthal coverage did not introduce important variation in the inversion results, both concerning the CLVD percentage and the fault plane orientation. Results obtained by diminishing the number of stations used and using a wrong earth model (Fig. 5b), a wrong focal depth (Fig. 5c) and a wrong STF length (Fig. 5d) were similar to the ones obtained using data from the original configuration of eight stations with a homogeneous azimuthal coverage. Results obtained when applying a time domain inversion are shown on the right-hand side. These results are extremely important, as they show how both amplitude spectra and time domain inversion methods do not require a good azimuthal coverage. This is an important difference from the behaviour of other methods for focal mechanism determination.

4 APPLICATIONS TO EARTHQUAKES IN SPAIN

The method has been applied to seven shallow earthquakes which occurred in Spain (Fig. 6 and Table 1) in the period 2002–2005. The goal was to apply the method to a range of earthquakes with different characteristics and study possible problems, which can arise in the determination of seismic moment tensor. Selected events were chosen in order to differ in their epicentre location and presenting different problematic features, such as crustal heterogeneity (Gergal, event 1), bad azimuthal coverage (Alboran, event 2) and small magnitude down to M = 3.3 (Ripolles, event 3). Moreover, the different epicentre locations required the use of different crustal models for different earthquakes. In this study we considered the three horizontally layered earth models shown in Fig. 7: model M6 (Dañobeitia *et al.* 1998) was defined for Betic region, model M10 (Gallart *et al.* 1995) for the Alboran Sea, and model M11 (Institut Cartografic de Catalunya, ICC) for the Pyrenees area. Attenuation coefficients for all these models were taken from Pujades *et al.* (1990).

The Gergal earthquake occurred on 2002 February 4, with epicentre at 37.12°N and 2.53°W, and magnitude of $m_b = 5.1$ (Instituto Geográfico Nacional, IGN, Fig. 6 and Table 1). The depth was estimated in the range between 10 and 18 km by previous studies, such as in the catalogues from IAG, ETHZ, MEDNET and Harvard. Hypocentral studies from IGN and Rodriguez (2004) using *P* and *S* arrival times estimated a source depth of 9 and 10 km, respectively.

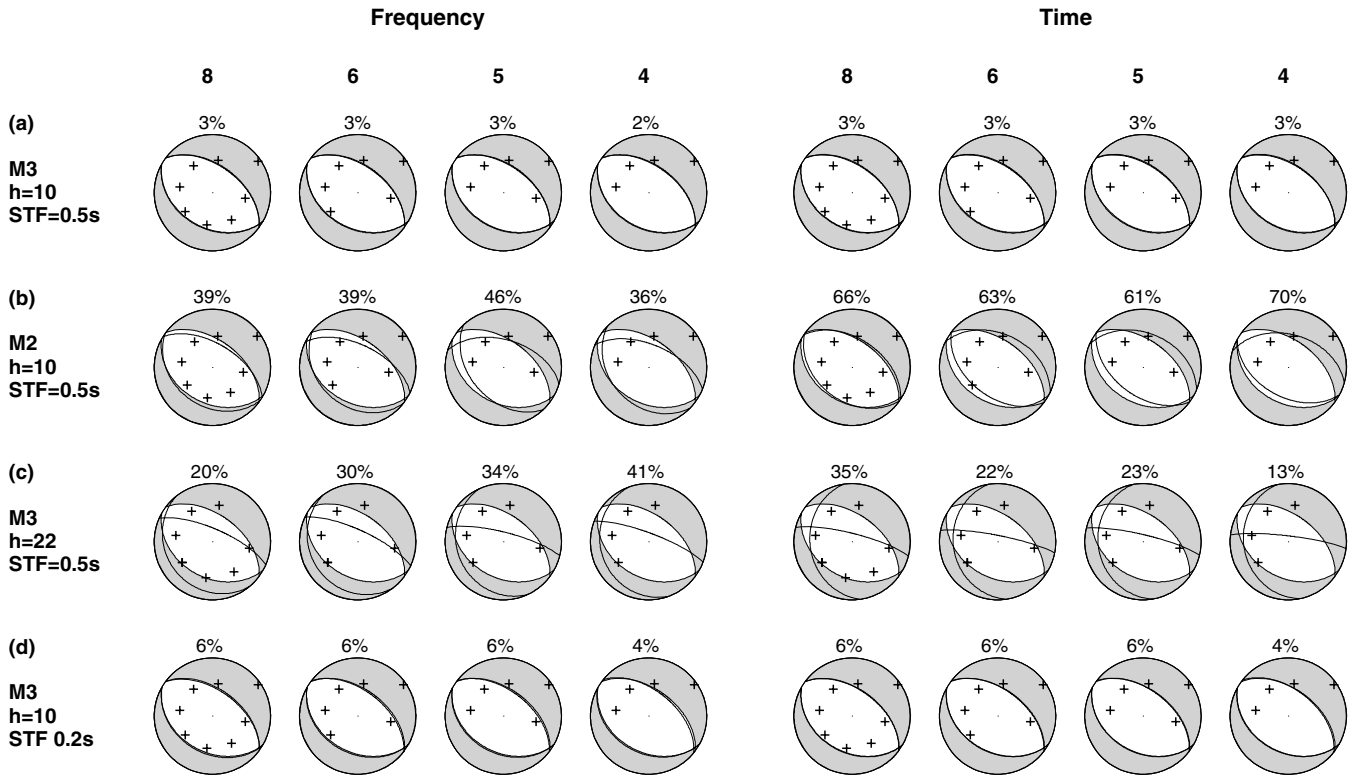

Figure 5. Results of amplitude spectra (left) and time domain (right) moment tensor inversion when reducing the azimuthal coverage. A total of 8, 6, 5 and 4 stations are used, respectively, for each column from left to right. Synthetic data have been generated with model M3, $h = 10$ km and STF of 0.5 s. Green functions have been obtained with the following different models: (a) model M3, focal depth 10 km and STF length of 0.5 s; (b) M2, $h = 10$ km, STF $= 10$ km; (c) M3, $h = 22$ km, STF $= 0.5$ s and (d) M3, $h = 10$ km, STF $= 0.2$ s. Each result is described by the correct focal mechanism used to generate synthetic data (grey focal sphere), DC component of the focal mechanism solution (black lines), CLVD percentage of solution and distribution of stations used (crosses).

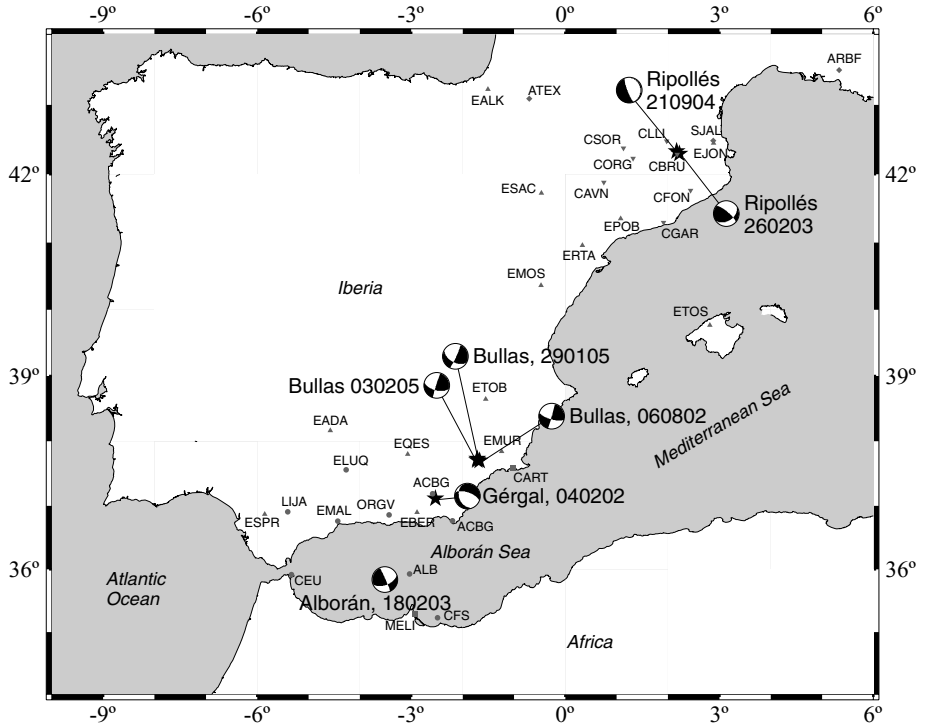

Figure 6. Location and focal mechanism (DC component) of the earthquakes studied: 1. Gérgal (2002/2/4), 2. Alborán (2003/2/19), 3. Ripollés (2003/2/26), 4. Ripollés (2004/9/21), 5. Bullas (2002/8/6), 6. Bullas (2005/1/29) and 7. Bullas (2005/2/3). Broad-band stations used belong to the following networks: ROA/UCM/GFZ (squares), IGN (triangles), ICC (inverse triangles), ReNaSS (diamonds) and TEDESE temporal network (circles). The station code is plotted.

Table 1. Summary of the earthquakes studied: event name, origin time, latitude and longitude, number of stations used for the inversion (number of stations used for polarities comparison are shown between brackets when different), strike, dip and slip of the fault planes, percentage of CLVD, focal depth, scalar seismic moment, magnitude M_w, STF duration and frequencies of the bandpass filter.

Event	Date, Time	Lat., Lon.	Stations	Strike, Dip, Slip	CLVD	Depth (km)	M_0 (N m)	M_W	STF (s)	f (Hz)
1. Gergal	02/02/2004 20:09:30.4	37.12°N 2.57°W	12 (11)	152°, 36°, −50°; 286°, 63°, −115°	4 per cent	9	0.86×10^{16}	4.6	0.8	0.1–2
2. Alboran	2003/2/18 13:09:37.7	35.84°N 3.53°W	11 (12)	70°, 57°, −12°; 166°, 80°, −147°	9 per cent	3	2.61×10^{16}	4.9	1.0	0.1–2
3. Ripolles	2003/2/26 3:32:57.5	42.30°N −2.22°W	10	57°, 44°, 34°; 302°, 67°, 129°	1 per cent	7	0.85×10^{14}	3.3	0.5	0.5–4
4. Ripolles	2004/9/21 15:48:04.8	42.34°N −2.17°W	12 (14)	15°, 9°, −57°; 162°, 83°, −95°	41 per cent	4	0.93×10^{15}	4.0	0.5	0.5–4
5. Bullas	2002/08/06 6:16:19.0	37.54°N 1.50°W	9	106°, 71°, −179° 16°, 89°, −19°	2 per cent	4	0.78×10^{16}	4.5	1.0	0.1–2
6. Bullas	2005/01/29 7:41:31.0	37.88°N 1.78°WE	10	119°, 52°, −173° 25°, 84°, −38°	5 per cent	4	1.54×10^{16}	4.7	1.0	0.1–2
7. Bullas	2005/02/03 11:40:33.0	37.82°N 1.79°W	10	105°, 59°, 176°; 197°, 87°, 31°	17 per cent	3	0.74×10^{15}	3.8	0.5	0.1–2

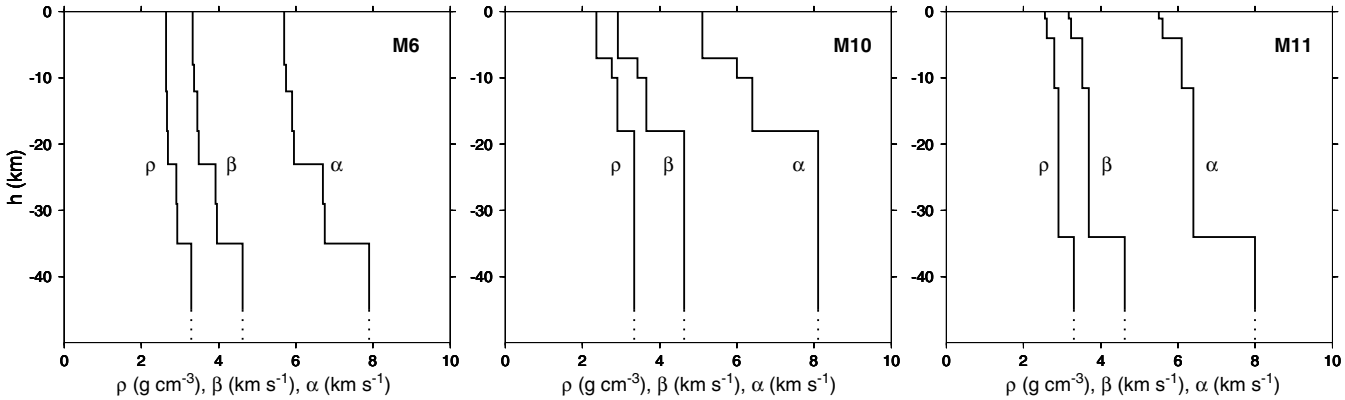

Figure 7. Crustal models used for moment tensor inversion of shallow earthquakes in Spain: model M6 (Dañobeitia *et al.* 1998, Betics region), M10 (Gallart *et al.* 1995, Alboran sea) and M11 (ICC, Pyrenees region). Density (ρ), P (α) and S wave velocities (β) versus depth are plotted.

We used vertical and radial components of P waves, as well as transverse components of S waves for 12 broad-band stations at regional distances ($\Delta < 350$ km), applying a bandpass filter between 0.1 and 2 Hz. Owing to the heterogeneity of the crustal structure in this region and the availability of different layered models (Mezcua & Martínez Solares 1983; Gallart *et al.* 1995; Dañobeitia *et al.* 1998), the moment tensor was calculated for several different sets of earth models. Best results were found with model M6 (Fig. 7, Dañobeitia *et al.* 1998). A test to reproduce better the lateral heterogeneities, by using a specific crustal model for the Alboran Sea (model M10, Fig. 7) at stations ALB (Alboran Island), CEU and CFS (African coast), did not improve the results. The inversion algorithm determined possible solutions for a range of depths between 1 and 19 km. While in theoretical tests the best solution was easily identified, results for Gergal earthquake show a more complex pattern. In particular, we observed two sets of solutions (grey and black dots in Fig. 8), each of them constituted of possible solutions (local or global minima) of similar focal mechanism and obtained for different source depths. If we simply base the selection of the best solution on the fit of observed amplitude spectra, we will obtain the misfit versus depth curve shown in Fig. 8(a) (top) and, therefore, select solutions in the range of 8–10 km from the first set (grey dots). Nevertheless, these solutions are characterized by very high CLVD percentages (up to 76–82 per cent at 8–10 km depth), which are uncommonly high for small-to-moderate tectonic earthquakes. The plot of CLVD component versus depth (Fig. 8a, centre) indicates an alternative family of best solutions (black dots), which minimizes the non-DC component at 9–10 km depth. The introduction of the combined misfit (eq. 6) solves the ambiguity and is indicating the best solution in a depth of 9 km corresponding to a normal focal mechanism with a small CLVD (4 per cent). The plot of the DC component of the focal mechanism, together with the alternative solutions at the same depth is shown in Fig. 8(b). The solution is consistent with most of the first motion polarities. Variation of STF length leads to a further small improvement (Fig. 8c, Table 1) for a source duration of 0.8 s. The estimated scalar seismic moment is 0.86×10^{16} N m, corresponding to a magnitude $M_w = 4.6$. The plot of observed and theoretical spectra for this solution is shown in Fig. 9 (left), the amplitudes having been rescaled to a common epicentral distance of 100 km. By scaling the amplitudes, characteristics of radiation pattern can be more clearly observed: as an example, low amplitudes at station ACBG indicate this is a nodal station. In general synthetic spectra may reproduce the main features of data and the amplitude variation related to the radiation pattern. The vertical (and radial) component of the observed spectra have a better fit than the transverse ones, where synthetic spectra show

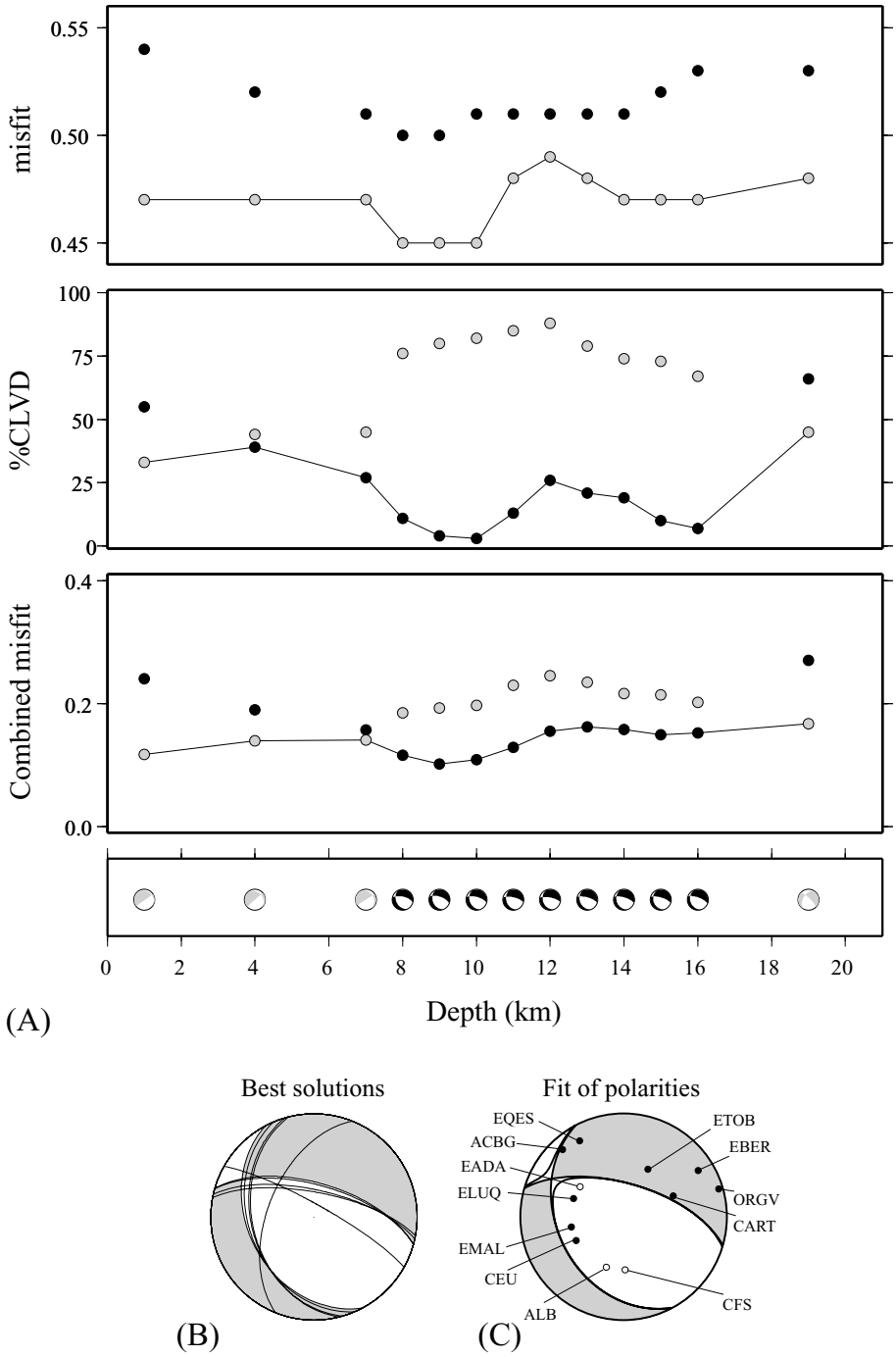

Figure 8. Summary of results of the inversion for Gérgal earthquake (2002/2/4). (a) Plot of misfit versus depth (top), CLVD versus depth (middle) and combined misfit versus depth (bottom) for two sets of solutions (grey and black dots). (b) Comparison of best solutions obtained by considering the combined misfit for a depth of 9 km. the focal mechanism of the DC component is plotted for all solutions which present a combined misfit up to 10 per cent higher than the one of best solution. (c) Comparison between observed first motion polarities (black and white dots corresponding to compression and dilatation) and the best solution obtained minimizing the combined misfit (DC+CLVD).

higher amplitudes with respect to the observed ones. The fit of amplitudes is also difficult at IGN stations, which are often located at larger epicentre distances. Although the inversion fits the spectra only, it is interesting to present the comparison between theoretical and observed seismograms (right-hand side of Fig. 9). Theoretical seismograms fit 9 over 11 (82 per cent) observed polarities, being unable to explain polarities at stations ELUQ and EMAL, which lie westward of the epicentre, while at CEU data present too high noise level and the fit of polarity can not be established clearly. The figure shows how in many cases vertical components of theoretical seismograms can fit main features of the data (for example, at stations CART, ORGV, EBER and EMAL), while the transverse components of *S* waves are more difficult to reproduce, especially in terms of their amplitudes. Comparison of our results with solutions obtained by other authors (Fig. 10), such as the ones from Instituto Andaluz de Geofísica (IAG), MEDNET network, ETHZ and Harvard CMT

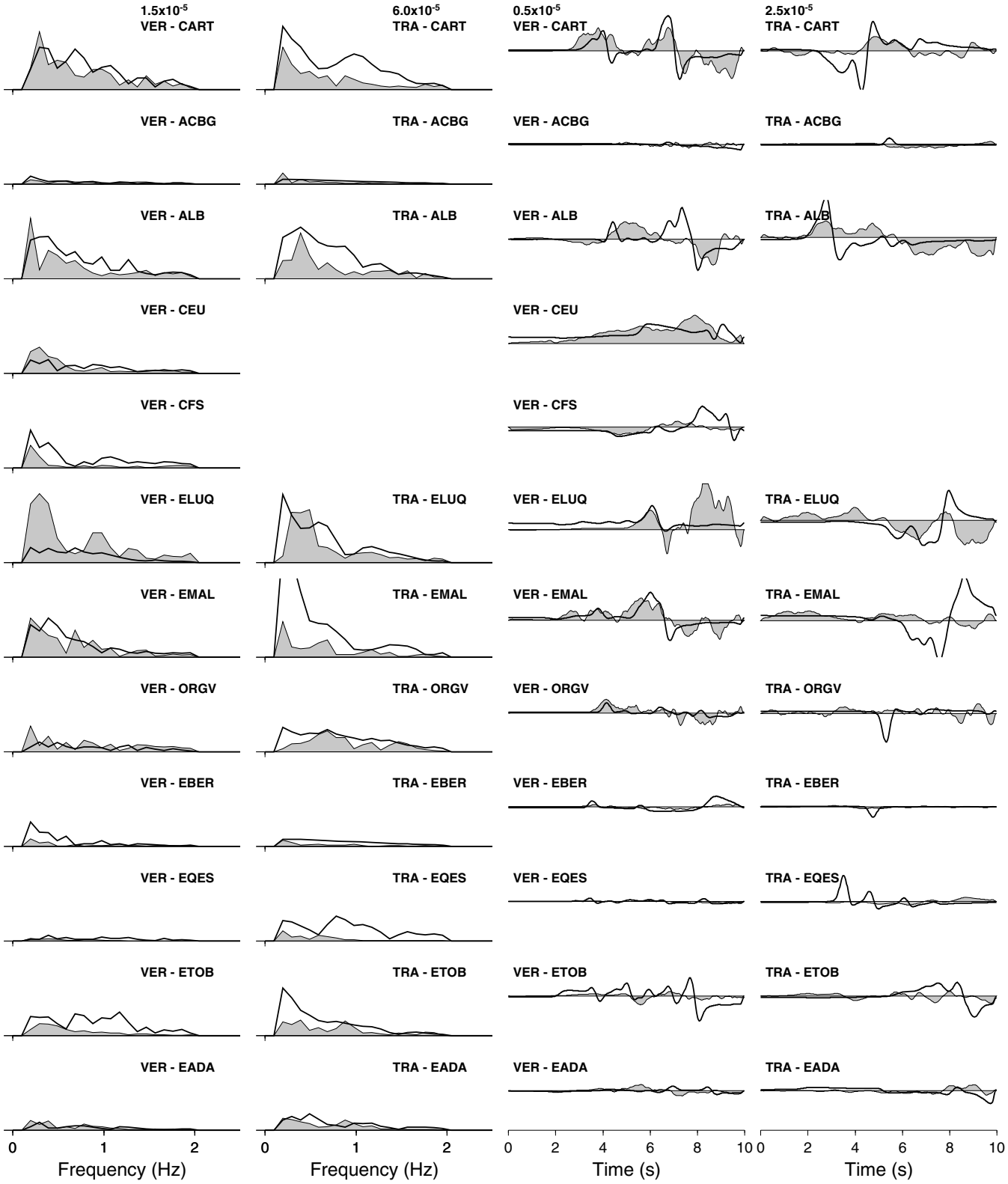

Figure 9. Comparison between observed (grey areas) and theoretical (black lines) amplitude spectra resulting from moment tensor inversion for the Gérgal earthquake (2002/2/4), for vertical and transverse components. Location of stations is shown in Fig. 8. The two right columns show the comparison between observed (grey areas) and theoretical (black lines) displacements, relatively to vertical and transverse components. All amplitudes are rescaled to a common epicentral distance of 100 km and normalized by coefficients shown at the top of each column.

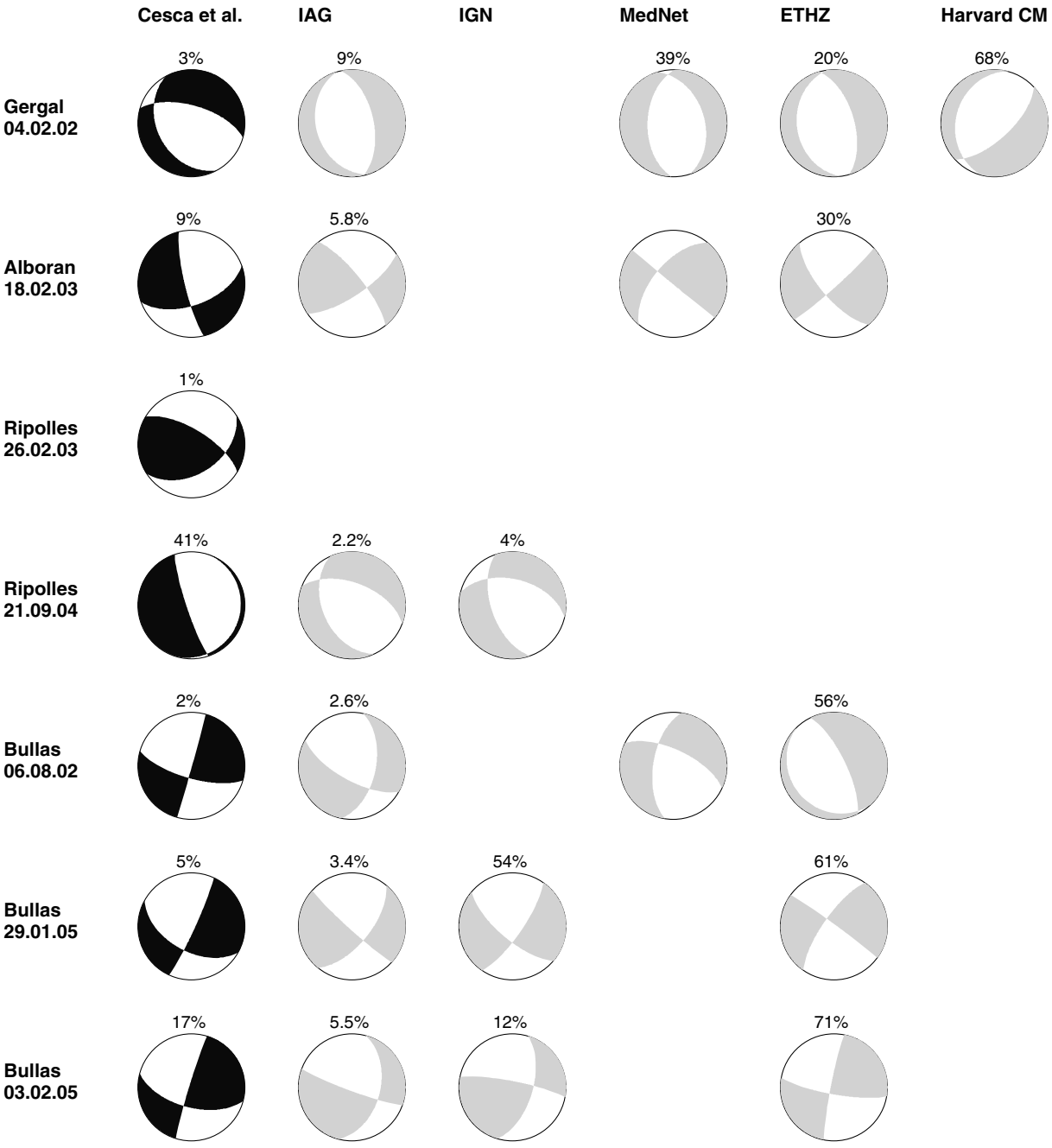

Figure 10. Comparison of available moment tensor inversion solutions for the seven earthquakes studied, including the plot of the DC component of the focal mechanism, percentage of the CLVD component, scalar seismic moment and focal depth.

catalogue shows agreement on a normal fault mechanism, but show in general smaller values of the strike angle. Some of these solutions, though, are characterized by high values of CLVD, such as MEDNET (39 per cent) or CMT (68 per cent). With respect to the source depth, the estimation of 9 km is in agreement with previous location studies (IGN; Rodriguez 2004) and the moment tensor inversion carried out by Stich *et al.* (2003), and smaller than the one obtained by the ETHZ ($h = 18$ km). The scalar seismic moment of 0.9×10^{16} N m ($M_w = 4.6$) is slightly lower than those from other solutions ($1.5–3.0 \times 10^{16}$ N m). We have related anomalies in the obtained solution, such as the appearance of two families of solutions and the impossibility of fitting some observed polarities, to the inaccuracy of our earth model description, which is unable to include the complexity of the crustal structure.

The Alboran earthquake (2003 February 18), which occurred at 35.84°N and 3.53°W, $m_b = 4.7$ (IGN), has been studied using the crustal model M10 (fig. 8, Gallart *et al.* 1995). This model presents a 3-layered crust, with a total thickness of 18 km, representing the Alboran Sea crustal structure. For the inversion procedure, we used vertical and radial components of *P* waves and transverse *S* waves, with a total of 11 broad-band stations and a bandpass filter between 0.1 and 2 Hz. We expected that the poor azimuthal coverage of the epicentre, mostly owing to the lack of stations in northern Africa, to be the most problematic feature for the inversion. Results of the

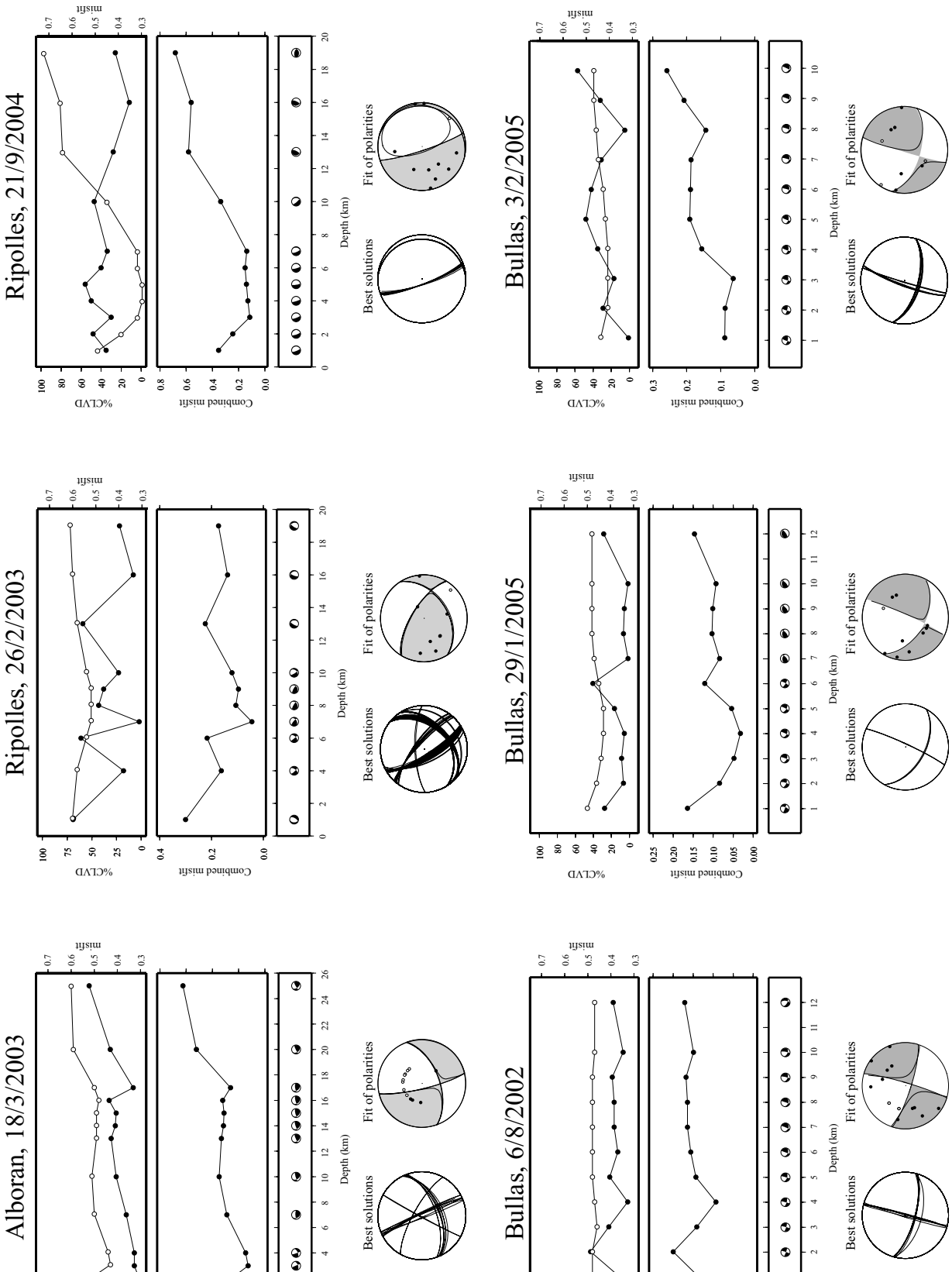

Figure 11. Summary of results of moment tensor inversion for the following earthquakes: 2. Alborán (2003/2/19), 3. Ripollés (2003/2/26), 4. Ripollés (2004/9/21), 5. Bullas (2002/8/6), 6. Bullas (2005/1/29), 7. Bullas (2005/2/3). Shown for each event are: plot of misfit (white dots) and CLVD percentage (black dots) versus depth, plot of combined misfit (black dots) versus depth and DC component of focal mechanism obtained at different depths. Below these plots are shown the comparison of DC components of solutions with best combined misfit (bottom left), and the comparison between observed first motion polarities (black and white dots) and the best solution (bottom right).

inversion are shown in Fig. 11 and are characterized by a more complex behaviour of misfit versus depth. A global misfit minimum is observed for 3–4 km and a second local minimum at 15–16 km depth. We think that the best solution corresponds to the global minimum, which also shows a smaller CLVD component and is confirmed by the analysis of combined misfit. This solution also presents a better fit of the observed polarities. Finally, the location of the epicentre in the Alboran Sea, with a crustal thickness of 18 km supports this conclusion of a very shallow hypocentre. Results are slightly improved when considering a different STF duration, corresponding to 1.0 s. With this parameter, the solution found (Table 1) for a depth of 3 km fits 10 over 11 of the observed polarities (91 per cent). The wrong polarity corresponds to station EMAL, which lie close to a nodal plane. The polarity also fits at station MELI, which is south of the epicentre; data from this station were not used for the inversion, owing to high noise levels. The obtained moment tensor corresponds to a strike-slip mechanism, in agreement with solutions proposed by other authors (Fig. 10). Our source depth is similar to the one proposed by IAG ($h = 4$ km) and lower than the solution obtained by ETHZ ($h = 12$ km), which is characterized by a CLVD component of 30 per cent. We think the determination of a depth of 28 km by MEDNET is excessive, considering the small thickness of the crust in the region. The scalar seismic moment, here 2.6×10^{16} N m ($M_w = 4.9$), agrees with all other solutions, which range between 2.0×10^{16} and 3.3×10^{16} N m. We observed here some instabilities with the depth estimation, as the double minimum, but our final results still prove that the method is capable of retrieving a good solution even with poor azimuthal station coverage.

We have studied two earthquakes which occurred in the Ripolles region in 2003 and 2004 (Fig. 6, Table 1). The first shock occurred on 2003 February 26, with a source depth estimated in 6 and 7 km, by IGN and ICC, respectively. The small magnitude ($m_b = 3.8$) of this event represents the most problematic feature for the moment tensor inversion and requires taking into account higher frequencies components of the waveform. We used 10 broad-band stations for the inversion. We obtained Green functions for all stations for a four-layered crustal model M11 (Fig. 7), which is normally used at ICC for epicentre location in this region. The inversion procedure used vertical components of *P* waves and transversal components of *S* waves. After the spectral analysis of the seismic *P* and *S* waves, which indicated the excitation of higher frequencies compared with those of the earthquakes previously studied, we applied a bandpass filter between 0.5 and 4 Hz to the seismograms and Green functions. Results of moment tensor inversion for a range of shallow source depths are shown in Fig. 11: the source depth is estimated in 7 km, in agreement with values obtained by IGN and ICC. The solution corresponds to a strike-slip to reverse faulting earthquake, and the CLVD component is equal to 2 per cent. We checked several STF durations in the range 0.3–0.5 s and the best solution was obtained for 0.5 s (Fig. 11, Table 1). This solution represents a nearly pure DC mechanism (CLVD = 1 per cent), scalar seismic moment being equal to 0.85×10^{14} N m ($M_w = 3.3$). This solution fits all the observed polarities (Fig. 11). Our focal mechanism also agrees with stress field studies for this area of Catalunya (Goula *et al.* 1999), while there are no solutions proposed in moment tensor catalogues. Good results obtained by the amplitude spectra inversion with the seismic data of the Ripolles earthquake prove the capacity of the method to determine moment tensors even for small earthquakes, when a correct crustal model is selected and a test over different depths is carried out. Fig. 12 shows the comparison between observed and theoretical amplitude spectra and displacements, which are again rescaled to a common distance of 100 km. Note that only amplitude spectra have been fitted. The inversion method has been applied to a second earthquake which occurred in the same region on 2004 September 21, with a magnitude of $m_b = 4.1$ (Table 1 and Fig. 6). We used data from 11 broad-band stations at regional distances. Three more stations in France (ATEX, SJAL, ARBF) were included only for comparison of first motion polarities. We carried out the inversion procedure with the same parameters, earth model and filter applied as for the study of the first Ripolles earthquake. Results of moment tensor inversion (Fig. 11) show a different focal mechanism, corresponding to a vertical fault and a source depth of 4 km. The variation of STF duration leads to minor changes in the focal mechanism and the scalar seismic moment. The best solution (Fig. 11, Table 1) was obtained for a STF length of 0.5 s. The scalar seismic moment is equal to 0.93×10^{15} N m ($M_w = 4.0$). The comparison with observed polarities shows agreement at 12 of 14 stations (86 per cent); the solution can not fit polarities at the nodal station CLLI and at station CBRU, which we relate to the small epicentral distance. The solution is mainly characterized by an anomalous percentage of the non-DC component (CLVD = 41 per cent). The low quality of mechanism resolution for this earthquake is consistent with differences from solutions proposed by other authors (Fig. 10). Results of theoretical tests suggest that this may be due to instabilities of the moment tensor inversion procedure for a source very close to the free surface ($h = 4$ km).

A last application of moment tensor inversion included three earthquakes, which occurred in 2002 and 2005 in the Murcia region (Fig. 6, Table 1), close to the village of Bullas, where the 2005 main event caused serious damage to buildings and structures in the area (Buforn *et al.* 2006). The first earthquake occurred 2002 August 6 (magnitude $M_W = 4.5$), while the others two were the main shock and its major aftershock at the beginning of 2005 (on 2005 January 29 and 2005 February 3, with magnitudes $M_W = 4.7$ and $M_W = 3.8$). Depending on the earthquake, we could use 9 or 10 broad-band stations at regional distances. We calculated theoretical Green functions for model M6 (Fig. 7) and carried out the inversion procedure with the same parameters as for the Gergal earthquake. Mayor results, including plots of misfit, CLVD and combined misfit versus depth are shown in Fig. 11 for each event. In the same figure, the comparison of the best solutions and the fit of the observed polarities is shown. Best solutions for the three earthquakes are very similar, indicating a strong relation to a possible major faulting system. Focal mechanisms (Table 1) are characterized by a major component of strike-slip mechanism, the percentage of CLVD being relatively small (2, 5 and 17 per cent in the three cases). For the two events which occurred in 2005, these results are in good agreement with solutions proposed by other authors (Fig. 10). There is no such agreement for the 2002 Bullas earthquake. Fig. 10 shows a set of different proposed source mechanism for this event. The IGN solution, which is based on the fit of observations at a smaller number of stations (3), shows a large component of CLVD (54 per cent) for the Bullas 2005 main shock, similar to the values obtained by the ETHZ for the 2002 and 2005 events (56 and 61 per cent, respectively). Still, it is important to observe the similarity of moment tensor solutions obtained in this study for the 2002 and 2005 earthquakes. Estimated source depths are also very similar, being 3 to 4 km. These values are consistent with hypocentral locations by IGN. We stress that the focal depth determination is well constrained for the two more recent events, while it is difficult to resolve for the 2002 event, for which the variation of the misfit as a function of depth is not significant (Fig. 11). Best solutions correspond to a STF of 1.0 s in the case of the two main events (in 2002 and 2005), and 0.5 s for the 2005 aftershock, with scalar

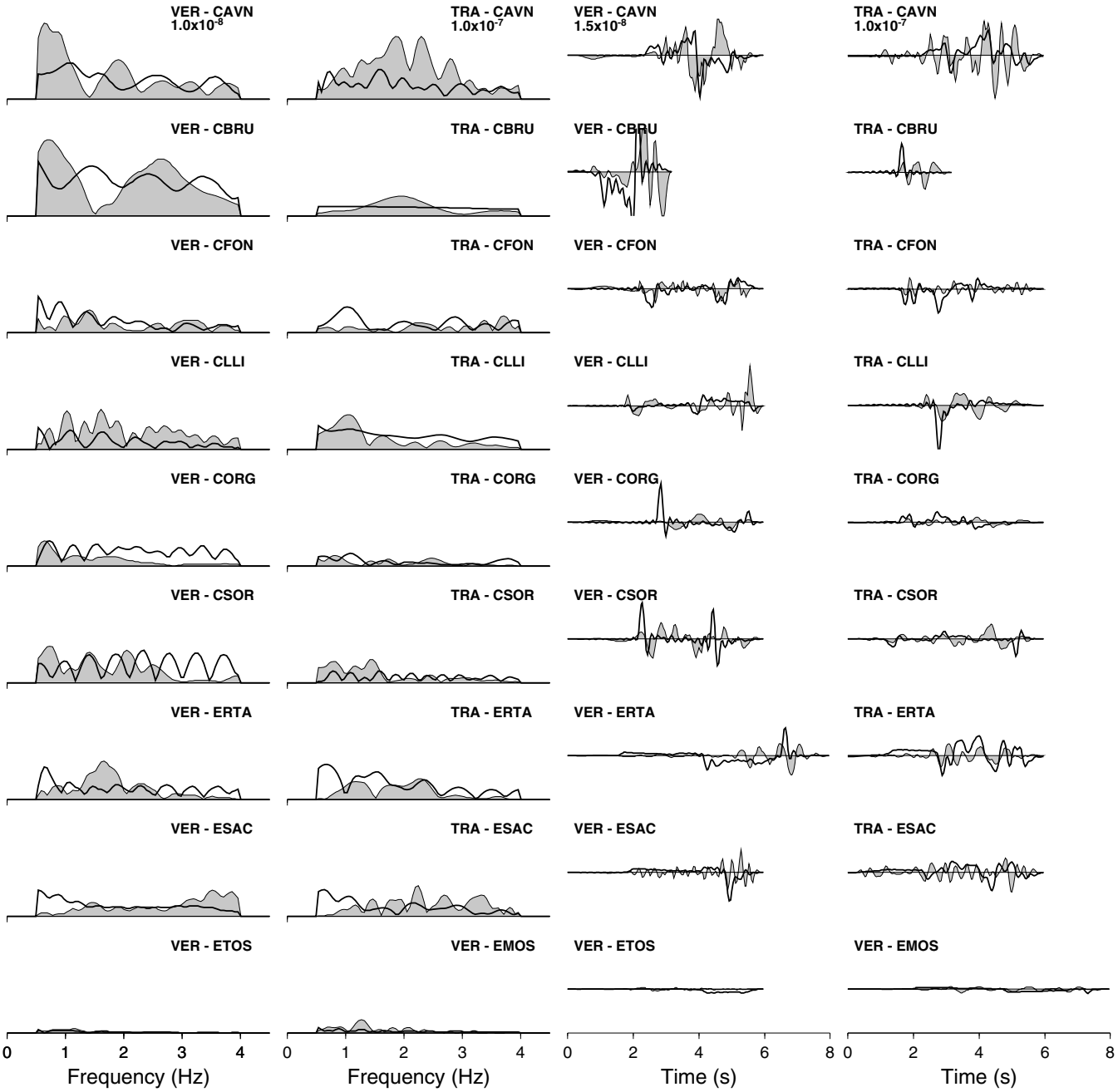

Figure 12. Comparison between observed (grey areas) and theoretical (black lines) amplitude spectra resulting from moment tensor inversion for the Ripolles earthquake (2003/2/26), for vertical and transverse components. The two right columns show the comparison between observed (grey areas) and theoretical (black lines) displacements, relative to vertical and transversal components. All amplitudes are rescaled to a common epicentral distance of 100 km and normalized by coefficients shown at the top of each column.

seismic moment values equal to 0.78×10^{16} N m ($M_w = 4.5$) and 1.54×10^{16} N m ($M_w = 4.7$), for the two main shocks in 2002 and 2005, and 0.74×10^{15} N m ($M_w = 3.8$) for the 2005 aftershock. The comparison with observed first motion polarities is correct in the 85, 89 and 86 per cent of the cases, respectively.

5 CONCLUSIONS

An amplitude spectra moment tensor inversion has been successfully applied to the study of focal mechanisms of shallow earthquakes at regional distances by using broad-band seismic data. Synthetic data case analysis allowed a careful study of the effects of a wrong modelling on the quality of solution for moment tensor inversion, showing how this depends strongly on both model layering and source depth definition. Both parameters have a great influence on results, and a wrong solution can be due to a wrong definition of either of them. Anomalously high CLVD components, which can be obtained as results of the moment tensor inversion, may be due to an incorrect earth model or focal depth. Both parameters are correlated and should be studied carefully. On the other hand, an accurate definition of STF duration has a minor influence on the moment tensor

determination, its mayor effect being in the estimation of the scalar seismic moment. A reduction of the azimuthal coverage also has a minor impact on the results of the inversion. As a general conclusion from these synthetic tests, we can observe that simplifications introduced by the modelling of a complex crustal structure may result in anomalous solutions and, therefore, special care is required in the interpretation of results. As a guideline to solve ambiguities in this interpretation, such as the appearance of multiple local minima, we propose a modified misfit definition, which is weighted by the fit of amplitude spectra, DC solution and first motion observed polarities.

The application of the proposed methodology to different shallow earthquakes in Spain brought satisfactory results, independent of the significant litospheric heterogeneities, which characterize the different source regions (Eastern Betics, Alboran See, Pyrenees). Results generally show good agreement with some solutions presented by other authors, both in terms of the focal mechanism and the source depth. The quality of focal mechanisms retrieved is also supported by their agreement with observed first motion polarities. These applications resulted in an analysis of the capability of the method with seismic data from regional distances and confirmed the importance of an optimal selection of the crustal model and the source depth. As a consequence, the comparison of results for several earth models with a range of source depth is required to define the best solution. A better determination of the focal mechanism in heterogeneous regions, such as southern Spain, may also require taking into account different earth models for the calculation of Green functions at different stations, or may require full 3-D models. When the crustal model is well defined, the amplitude spectra inversion can determine moment tensor components, even in the case of small earthquakes with magnitude $M_W < 3.5$, such as the first Ripollés event, and even with poor azimuthal coverage of the epicentre (Alborán earthquake, with an azimuth gap larger than 220°). However, when studying complex regions with important lateral heterogeneities in crustal structure, as is the case of the Gergal earthquake, the misfit to data may be high and multiple local minima may exist. In this case, adding the information of fitted polarities or taking into account the amount of the DC component in the misfit function (combined misfit) is useful.

In this study an alternative method for the inversion of the moment tensor for the mechanism of shallow earthquakes is defined. The inversion approach, which is carried out in the frequency domain and use only body waves here, differs from the majority of studies applied to the region (Dziewonski & Woodhouse 1983; Braunmiller *et al.* 2002; Pondrelli *et al.* 2002; Stich *et al.* 2003); these work in the time domain and use data from surface waves or filter the high-frequency content of the seismograms. Our approach in the frequency domain presents some advantages. First, it is less dependent on a precise data alignment and is in general more stable than the time domain approach. Another important advantage of the method is that, by fitting amplitude spectra of body waves, it can be used successfully for the inversion of small earthquakes, or in case of deeper earthquakes which excite small amplitude surface waves. Using body waves gives the possibility to consider different crustal structures at the source and receiver by means of a reflectivity Green functions (e.g. code of Wang 1999). The proposed method is suitable for fast moment tensor calculation. To this goal, a Green function database generator has recently been implemented, capable of dealing with different crustal models and source depths. This procedure has already been tested in the study of seismic events in North Iceland, being extremely helpful in reducing computational times, as the calculation of Green function is the most time consuming step in the proposed method.

ACKNOWLEDGMENTS

This work has been partially funded by the Ministerio de Educacion y Ciencia of Spain (FPU grant AP2000-3603 and project REN2003-05178-C03, ERSE) and by the SPICE project (Contract Number MRTN-CT2003-504267) of the European Commission's Human Resources and Mobility Program. We would like to thank Dr D. Stich and an anonymous reviewer for their suggestions, and Prof. L. Drake for revising the English text.

REFERENCES

Aki, K. & Richards, P.G., 1980. *Quantitative Seismology: Theory and Methods,* W.H. Freeman and Co., San Francisco, California.

Braunmiller, J., Kradolfer, U., Baer, M. & Giardini, D., 2002. Regional moment tensor determination in the European-Mediterranean area: initial results, *Tectonophysics*, **356,** 5–22.

Brüstle, W. & Müller, G., 1983. Moment and duration of shallow earthquakes from Love-wave modelling for regional distances, *Phys. Earth planet. Inter.,* **32,** 312–324.

Buforn, E., Udias, A. & Mezcua, J., 1988. Seismotectonics of the Ibero-Magrebian region, *Tectonophysics,* **248,** 247–261.

Buforn, E., Udías, A. & Madariaga, R., 1991. Intermediate and deep earthquake in Spain, *Pure Appl. Geoph.,* **136,** 375–393.

Buforn, E., Sanz de Galdeano, C. & Udías, A., 1995. Seismotectonics of the Ibero-Maghrebian region, *Tectonophysics,* **248,** 247–261.

Buforn, E., Coca, P., Udías, A. & Lasa, C., 1997. Source mechanism of intermediate and deep earthquakes in southern Spain, *J. Seism.,* **1,** 113–130.

Buforn, E., Bezzeghoud, M., Udias, A. & Pro, C., 2004. Seismic sources on the Iberia-Africa plate boundary and their tectonic implications, *Pure appl. Geophys.,* **161,** 623–646.

Buforn, E., Cesca, S., Goded, T., del Fresno, C. & Muñoz, D., 2006. The Bullas (Murcia, SE Spain) January 29, 2005 earthquake, *J. Seism.,* **10,** 65–72.

Calvert, A. et al., 2000. Geodynamic evolution of the litosphere and upper mantle beneath the Alboran region of the western Mediterranean: constraints from travel time tomography, *J. geophys. Res.,* **105,** 10 871–10 898.

Cesca, S., 2005. Inversión del tensor momento sísmico de terremotos superficiales a distancias regionales, *PhD thesis*, Universidad Complutense de Madrid, Spain, 289 pp.

Coca, P., 1999. Métodos para la inversión del tensor momento sísmico. Terremotos del Sur de España, *PhD thesis,* Universidad Complutense de Madrid, Spain, 300 pp.

Dahm, T. & Krüger, F., 1999. Higher degree moment tensor inversion using far-field broadband recordings: theory and evaluation of the method with application to the 1994 Bolivia deep earthquake, *Geophys. J. Int.,* **137,** 35–50.

Dahm, T., Manthei, G. & Eisenblätter, J., 1999. 'Automated moment tensor inversion to estimate source mechanisms of hydraulically induced microseismicity in salt rock', *Tectonophysics,* **306,** 1–17.

Dañobeitia, J.J., Sallares, V. & Gallart, J., 1998. Local earthquake seismictomography in the Betic Cordillera (southern Spain), *Tectonophysics,* **160,** 225–239.

Dreger, D.S. & Helmberger, D.V., 1993. Determination of Source Parameters at Regional Distances with Single Station or Sparse Network Data, *J. geophys. Res.,* **98,** 8107–8125.

Dziewonski, A.M. & Woodhouse, J.H., 1983. An experiment in the systematic study of global seismicity: centroid moment-tensor solutions for 201 moderate and large earthquakes of 1981, *J. geophys. Res.,* **88,** 3247–3271.

Dziewonski, A.M., Chou, T.A. & Woodhouse, J.H., 1981. Determination of earthquake source parameters from waveform data for studies of global and regional seismicity, *J. geophys. Res.,* **86,** 2825–2852.

Gallart, J., Diaz, J., Vidal, N. & Dañobeitia, J.J., 1995. The base of the crust at the Betics-Alboran Sea transition: evidence for an abrupt structural

variation from wide-angle ESCI data, *Rev. Soc. Geol- España,* **8,** 519–527.

Goula, X., Olivera, C., Fleta, J., Grellet, B., Lindo, R., Rivera, L.A., Cisternas, A. & Carbon, D., 1999. Present and recent stress regime in the eastern part of the Pyreenes, *Tectonophysics,* **308,** 487–502.

Hatzfeld, D., 1978. Etude sismotectonique de la zone de collisione Ibéro-Maghrébine, *PhD thesis*, Université Scientifique et Médicale de Grenoble, France, 175 pp.

Jiménez-Munt, I. & Negredo, A.M., 2003. Neotectonic modelling of the western part of the Africa-Eurasia plate boundary: from the Mid-Atlantic ridge to Algeria, *Earth. planet. Sci. Lett.,* **205,** 257–271.

Jost, M.L. & Hermann, R.B., 1989. A Student's Guide to and Review of Moment Tensor, *Seism. Res. Lett.,* **60,** 37–57.

Kawakatsu, H., 1995. Automated near-realtime CMT inversion, *Geophys. Res. Lett.,* **22,** 2569–2572.

Koch, K., 1991. Moment tensor inversion of local earthquake data: I. Investigation of the method and its numerical stability with model calculations, *Geophys. J. Int.,* **106,** 305–319.

Mezcua, J. & Martínez Solares, J.M., 1983. *Sismicidad del Área Ibero-Magrebí,* Instituto Geográfico Nacional. Publicación 203, Madrid, Spain, 299 pp.

Müller, G., 1985. The reflectivity method: a tutorial, *J. Geophys.,* **58,** 153–174.

Morales, J., Serrano, I., Jabaloy, A., Galindo-Zaldivar, J., Zhao, D., Torcal, F., Vidal, F. & Gonzalez-Lodeiro, F., 1999. Active continental subdaction beneath the Betic Cordillera and Alboran Sea, *Geology,* **27,** 735–738.

Pondrelli, S., Morelli, A., Ekström, G., Mazza, S., Boschi, E. & Dziewonski, A.M., 2002. European-Mediterranean regional centroid-moment tensors: 1997-2000, *Phys. Earth planet. Inter.,* **130,** 71–101.

Pujades, L.G., Canas, J.A., Egozcue, J.J., Puigví, M.A., Gallart, J., Lana, X., Pous, J. & Casas, A., 1990. Coda-Q distribution in the Iberian Peninsula, *Geophys. J. Int.,* **100,** 285–301.

Rodriguez, I., 2004. Sismicidad y mecanismo focal de terremotos en el Sur de España: estudio de la determinación hipocentral e influencia de los errores, *DEA thesis*, Universidad Complutense de Madrid, Spain, 134 pp.

Rueda, J. & Mézcua, J., 2005. Near-real-time seismic moment-tensor determination is Spain, *Seism. Res. Lett.,* **76,** 455–465.

Sipkin, S.A. & Needham, R.E., 1993. Moment-tensor solutions estimated using optimal filter theory: global seismicity, *Phys. Earth planet. Inter.,* **75,** 199–204.

Souriau, A. & Pauchet, H., 1998. A new synthesis of Pyrenees seismicity ant its tectonic implications, *Tectonophysics,* **290,** 221–244.

Stich, D., Ammon, C.J. & Morales, J., 2003. Moment tensor solutions for small and moderate earthquakes in the Ibero-Maghreb region, *J. geophys. Res.,* **108**(B3), No. 2148.

Udías, A., 1999. *Principles of Seismology,* Cambridge University Press, Cambridge, UK.

Udías, A., Lopez Arroyo, A. & Mezcua, J., 1976. Seismotectonics of the Azores-Alboran Region, *Tectonophysics,* **31,** 259–289.

Wang, R., 1999. 'A simple orthonormalization method for stable and efficient computation of Green functions', *Bull. seism. Soc. Am.,* **89,** 733–741.